Predictions of Endwall Losses and Secondary Flows in Axial Flow Turbine Cascades

O. P. Sharma
Senior Research Engineer.

T. L. Butler
Project Engineer.

Engineering Division,
Pratt & Whitney Aircraft Group,
East Hartford, CT 06108

This paper describes the development of a semi-empirical model for estimating endwall losses. The model has been developed from improved understanding of complex endwall secondary flows, acquired through review of flow visualization and pressure loss data for axial flow turbomachine cascades. The flow visualization data together with detailed measurements of viscous flow development through cascades have permitted more realistic interpretation of the classical secondary flow theories for axial turbomachine cascades. The re-interpreted secondary flow theories together with integral boundary layer concepts are used to formulate a calculation procedure for predicting losses due to the endwall secondary flows. The proposed model is evaluated against data from published literature and improved agreement between the data and predictions is demonstrated.

1 Introduction

A knowledge of the magnitude of losses is essential in the preliminary and detailed design phase of a turbomachine. Historically these losses have been divided into three distinct parts, namely profile losses, endwall secondary flow losses, and tip clearance losses. The profile losses are generated on the airfoil surfaces due to the growth of the boundary layers. These losses can be fairly accurately calculated in the detailed design phase for given airfoil surface static pressure distribution by using boundary layer calculation methods. It should be pointed out that a good transitional boundary layer calculation method and a model that accounts for the unsteadiness due to the rotor-stator interaction is essential if reliable estimates of profile losses in a rotating rig environment are to be obtained. For a given family of airfoils designed for prescribed velocity triangles, profile losses can also be fairly accurately estimated in the initial phase of the turbine design. The magnitudes of endwall secondary flow losses and tip leakage losses, however, are almost exclusively obtained from available empirical correlations both in the initial and the detailed design phase of a turbomachine. Tip leakage losses mainly occur in rotors and these are invariably parasitic losses which can be reduced through active control of the tip clearance. The endwall secondary losses, on the other hand, occur because of the annulus wall boundary layers and their interaction with the airfoils in the blade row passage. Since these losses account for almost 30–50 percent of the total pressure loss in any blade row, it is important to understand the physical mechanisms responsible for generating these losses and to define a realistic formulation for estimating them which can be used for turbine designs.

Dunham [1] conducted a detailed review of the available correlations for endwall secondary flow losses and through his comparison with available data concluded that none of the then-existing methods gave a realistic estimate of losses for cascades. He proposed a correlation for the endwall secondary flow losses which was later modified by Came [2], Dunham and Came [3], and Morris and Hoare [4]. The modified formulation of Dunham's correlation is given by the following expression

$$Y=\frac{b}{h}\frac{\sin\beta_2}{\sin\beta_1}\left(\frac{C_L}{\tau/b}\right)^2\frac{\sin^2\beta_2}{\sin^3\beta_m}\left(0.294\frac{\delta^*}{b}+0.011\right) \quad (1)$$

In his paper, Dunham concluded that a fresh approach to estimate endwall secondary flow by using three-dimensional boundary layer concepts was needed to get more realistic predictions of the endwall secondary flow losses.

A number of experimental investigations [5–9] have been conducted over the past decade in large-scale rectilinear and annular cascades to provide more insight into the complex three-dimensional flows in the endwall regions and to provide a data base to facilitate three-dimensional endwall boundary layer and/or three-dimensional viscous flow calculations. Sieverding [10] gave an excellent review of these recently conducted studies in order to outline the state-of-the-art understanding of the basic aspect of the secondary flows in turbine blade passages. In his paper, Sieverding provided detailed insight into the topology of the complex three-dimensional flow field in the endwall regions; however, he did not provide any viable procedure to estimate endwall losses.

To the authors' knowledge, only two endwall loss prediction methods [11, 12] have appeared in the literature since Dunham's correlation which can be used in turbine design process. The formulation provided by Gregory-Smith [11] allows estimation of both the spanwise distribution of endwall losses and the exit air angle deviation due to secondary flow. However, this method can be used only in the detailed design process where airfoil shapes and flowpath geometry have been

Contributed by the Gas Turbine Division of THE AMERICAN SOCIETY OF MECHANICAL ENGINEERS and presented at the 31st International Gas Turbine Conference and Exhibit, Düsseldorf, Federal Republic of Germany, June 8–12, 1986. Manuscript received at ASME Headquarters February 14, 1986. Paper No. 86-GT-228.

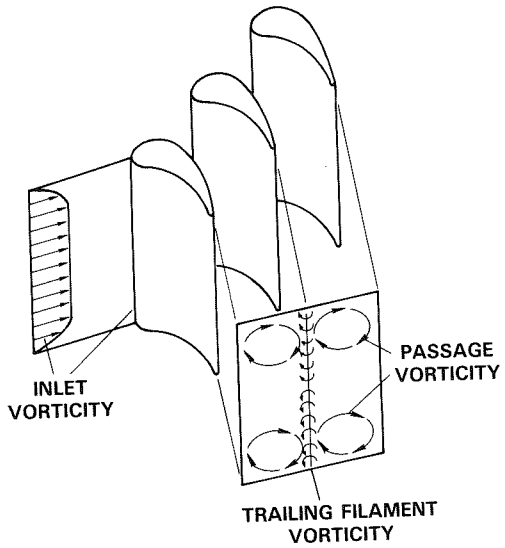

Fig. 1 Cascade vorticity as predicted by classical secondary flow theories

defined. The correlation of Mukhtarov and Krichakin [12] can be used in the initial design phase where optimization and selection of turbine parameters and flow path are being conducted. It should also be pointed out that a number of viscous numerical calculation methods [13, 14, 33] have been developed over the past 15 years which have the potential to influence the optimization of turbines once realistic turbulence models capable of predicting three-dimensional transitional flows become available. These state-of-the-art numerical methods can only be used to guide experimental work and designs at the moment.

The primary objective of the present paper is to demonstrate that the detailed data obtained in the last 15 years have provided sufficient information about the endwall secondary flows in turbine cascades to allow a physically realistic model for the endwall secondary flow losses. In addition, these data have also provided new insight about the effect of inlet boundary layer (normal component of vorticity) on the secondary flow which indicates that the classical approach of inviscid secondary flow theory originally proposed by Squire and Winter [15], and subsequently generalized and applied by many investigators [16–19], may yield misleading results as far as endwall secondary flows in turbomachine cascades are concerned unless proper care is taken while applying these theories. A description of the flow field in the endwall region of turbine cascades is given below with special reference to the effect of inlet boundary layer to substantiate the above statement.

2 Flow Structure in the Endwall Region

An extensive amount of theoretical and experimental work has been conducted over the past forty years to understand and estimate secondary flows in axial turbomachine cascades. Until the recent availability of three-dimensional viscous codes, most of the theoretical work has concentrated on developing and applying inviscid secondary flow theories. The secondary flow vortex system predicted by these classical secondary flow theories is shown in Fig. 1 as described by Hawthorne [16]. It shows the resulting component of exit vorticity in the direction of the flow when fluid with inlet vorticity is deflected through a cascade. Three distinct mechanisms contribute to the secondary vorticity at the exit of the cascade:

(*i*) distributed secondary vorticity which appears as the passage vortex at the exit of the cascade which is generated by the distortion of the vortex filaments of the inlet boundary layer as it passes through a curved passage;
(*ii*) trailing filament vorticity which is generated due to the stretching of the inlet vortex filaments when passing through the cascade with different velocity between the suction and the pressure side;
(*iii*) trailing shed vorticity which is generated due to the spanwise change of the blade circulation.

A number of expressions are available for calculating the distributed secondary vorticity. Almost all of these expressions have been derived by assuming that the flow in the cascade passage is frictionless. These expressions have provided surprisingly good agreement with measured exit air angle data in cascades and curved ducts implying that viscous effects in cascades have a relatively small effect on secondary flows. It should, however, be pointed out that the energy losses estimated by using the theories are an order of magnitude smaller than those measured in cascades.

The sense of rotation of the trailing filament and the trailing shed vorticities are opposite to that of the distributed secondary vorticity and their relative contributions to the total secondary vorticity are much lower than the distributed secondary vorticity.

The secondary vorticity predicted by the classical secondary flow theories relies on the assumption that inlet boundary layer entering the cascade experiences flow turning in the passage resulting in distortion of vortex tubes which causes an

Nomenclature

B = constant
b = chord
bx = axial chord
CR = convergence ratio $\equiv \rho_2 U_2/\rho_1 U_1$
C_L = lift coefficient referred to vector mean velocity $\equiv 2(\tau/b)\,(\cot\beta_1 - \cot\beta_2)\sin\beta_m$
C_f = skin friction coefficient
h = height of the airfoil
H = boundary layer shape factor $\equiv \delta^*/\theta$
H^* = boundary layer shape factor $\equiv \delta^{**}/\theta$
M = Mach number
P_T = total pressure
P_s = static pressure
Ri = Richardson number $= \epsilon/\sqrt{CR}$
s = distance along the streamwise direction
TET = airfoil trailing edge thickness
U = velocity
Y = total pressure loss coefficient $\equiv (P_{Tref} - P_{T2})/(P_{Tref} - P_{S2})$
Z_{TE} = penetration height of the separation line on the airfoil suction surface at the trailing edge
β_m = vector mean air angle $= \cot^{-1}[\frac{1}{2}(\cot\beta_1 + \cot\beta_2)]$
β = gas angle measured from tangential
δ = boundary layer thickness
δ^* = boundary layer mass deficit thickness
δ^{**} = boundary layer energy deficit thickness
ϵ = gas turning in radians
θ = boundary layer momentum deficit thickness
ρ = density
τ = pitch of airfoils in cascades
$1-\phi^2$ = energy loss coefficient

Subscripts

1 = cascade inlet conditions
2 = cascade exit conditions

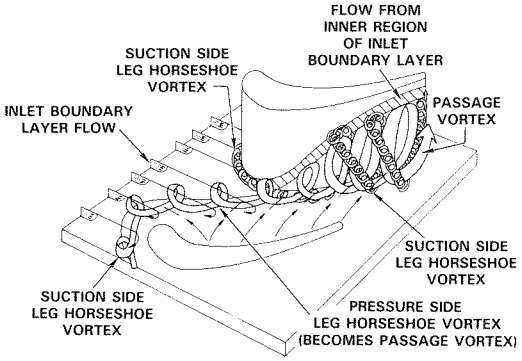

Fig. 2 Cascade endwall flow structure

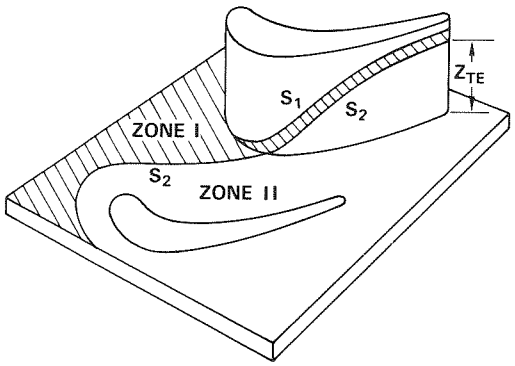

Fig. 3 Cascade endwall region separation lines

increase in vorticity in the streamwise direction. A review of the flow visualization and flow measurements in the leading edge region of cascade appears to dispute this assumption. Details of the flow field in cascades have been fairly well mapped by a number of recent investigators as discussed by Sieverding [10]. Figures 2 and 3 show flow patterns associated with the inlet boundary layer in a turbine cascade. This figure has been generated by utilizing available information from published literature [5, 9, 10, 20, 22, and 24] along with some additional insight obtained by the authors from some recently conducted experiments in full and large-scale cascade wind and water tunnels. As shown in the above figure, the boundary layer entering the cascade separates in the leading edge region forming a horseshoe vortex. A majority of the fluid from the inlet boundary layer gets trapped in this vortex which has two legs. These two legs are normally termed the pressure and the suction side legs. During this interaction the normal component of the vorticity associated with the inlet boundary layer is transformed into the streamwise component of vorticity as soon as the fluid enters the cascade before most turning of the mainstream flow has been achieved. The two legs of the horseshoe vortex entering the cascade are counterrotating, and if both contain equal amounts of fluid, then the net streamwise component of the vorticity would be zero in the exit plane of the cascade if the fluid in the cascade were frictionless. Recently conducted flow visualization tests at P&W indicate that the fluid particles closest to the wall in the cascade inlet boundary layer do not become part of the horseshoe vortex. These fluid particles get convected toward the suction side of the airfoil where they climb the airfoil surface exiting the airfoil on top of the passage vortex.

The pressure side leg of the vortex is immediately influenced by the blade-to-blade pressure gradient as it enters the passage and gets convected toward the suction side, meeting the surface near the minimum pressure point. Since all of the fluid particles from the inlet boundary layer have either become part of the horseshoe vortex or been convected toward the suction side, a new boundary layer starts at the endwall downstream of the separation line defined by the horseshoe vortex system.

As the pressure side leg of the vortex moves across the passage it entrains low-momentum fluid particles from this newly formed passage endwall boundary layer and it grows to become the passage vortex which is the most dominant feature of the flow. This entrainment of the passage endwall boundary layer fluid significantly affects the development of the passage vortex and is a key mechanism in the generation of the secondary flows and endwall losses. Since this mechanism is governed by viscosity one should not expect inviscid secondary flow theories to yield realistic magnitudes of secondary vorticity or endwall losses in cascades.

The suction side leg of the horseshoe vortex has a sense of rotation opposite to that of the pressure side leg of the vortex (and the passage vortex). It tends to follow the contour of the airfoil suction side remaining near the endwall until the point where the passage vortex interacts with the suction side of the airfoil. At this location, which is usually near the minimum pressure point in the cascade passage, the suction side leg of the vortex is forced off the endwall as it interacts with the passage vortex. As the flow proceeds downstream the suction side leg of the vortex orbits around the outside edge of the passage vortex retaining its identity. The location of this suction side leg of the vortex in the cascade exit plane depends on the size and vorticity associated with it and the passage vortex. The countervortex pointed out by Langston [5] at the airfoil suction surface endwall junction in the exit plane is most likely the suction side leg of the vortex which has arrived at the corner by spiraling around the passage vortex.

An important feature of the surface flow visualization on the endwall and the airfoil surfaces is the separation at reattachment lines, which was first identified by Langston [5] in a turbine cascade. Figure 3 shows the schematic of the surface flow visualizations. Zone I in the endwall region represents the region affected by the fluid particles which enter the cascade as the innermost part of the cascade inlet boundary layer. This fluid climbs the airfoil suction surface before the minimum pressure point and appears on the airfoil suction side between lines S1 and S2. The surface streamlines in zone II on the endwall indicate strong crossflows from the pressure to the suction side. This crossflow feeds the pressure side leg of the vortex and it grows to become the passage vortex. This separation line indicates the location where the pressure side leg of the vortex separates from the wall. This line meets the airfoil suction surface at the minimum pressure point and then climbs the airfoil suction surface. The height of the separation line S2 at the trailing edge of the airfoil approximates the diameter of the passage vortex. This line is one of the most prominent imprints of the endwall secondary flow vortex in the axial turbomachine passage. Knowledge of the penetration height of this separation line at the trailing edge on the airfoil suction surface can be used in estimating both endwall losses and secondary flows, as shown in the remainder of this paper.

3 Separation Line Penetration Height

Detailed review of a large body of available cascade data has indicated that the penetration of the separation line toward the midheight of the airfoil suction surface is a good indicator of the magnitude of secondary flow. The data of Langston et al. [5], Marchal and Sieverding [6], and Graziani et al. [9] show the region adjacent to the suction surface, between the separation line and the endwall, to be one of high loss and high external heat load associated with the passage vortex.

Because of the importance of the separation line as an indicator of heat loads and losses both for the midspan and endwall regions of the airfoil, extensive studies of cascade flow visualization experiments were conducted in order to develop

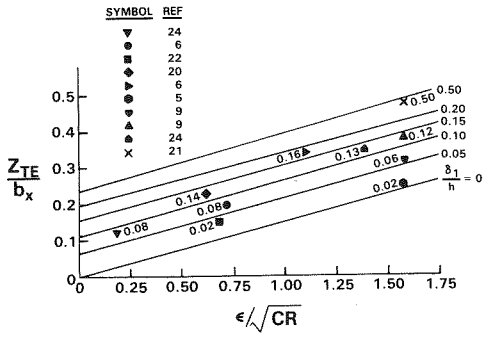

Fig. 4 Penetration height of the separation line on the airfoil suction surface at the trailing edge as a function of the cascade geometry and inlet boundary layer thickness

a correlation to predict its behavior. Figure 4 shows a plot of the penetration height of the suction surface separation line at the trailing edge as a function of cascade turning angle, convergence ratio and inlet boundary layer thickness. These data were obtained from surface flow visualizations reported in [5, 6, 9, 21, 22, 24]. The magnitude of the cascade inlet boundary layer thickness normalized by airfoil height is written next to each data point. The following expression gives a good estimate of the penetration height

$$\frac{Z_{TE}}{bx}=0.15\epsilon/\sqrt{CR}+f\left(\frac{\delta_1}{h}\right) \tag{2}$$

where Z_{TE} = penetration height of the separation line at the trailing edge on the airfoil suction surface; h = height of the airfoil; bx = axial cord; ϵ = flow turning angle in radians; CR = convergence ratio = $(\rho U)_{\text{exit}}/(\rho U)_{\text{inlet}}$; δ_1 = inlet boundary layer thickness.

The function $f(\delta_1/h)$ in the above expression can be approximated by

$$f\left(\frac{\delta_1}{h}\right)=1.4\frac{\delta_1}{h}-2.73\left(\frac{\delta_1}{h}\right)^2+1.77\left(\frac{\delta_1}{h}\right)^3 \tag{3}$$

It is noted that the curves for different inlet boundary layer thicknesses are parallel lines. This indicates that the increase in separation line penetration due to increasing boundary layer thickness is relatively independent of the cascade geometry (turning angle and convergence ratio). If one considers the penetration height of the separation line at the airfoil suction surface trailing edge to be an indicator of secondary flow, then this result contradicts various secondary flow theories [15–18]. These theories relate secondary vorticity at the exit of the cascade (due to inlet boundary layer) to the airfoil deflection (turning angle). However, these theories assume that the inlet boundary layer enters the cascade without interacting with the airfoil leading edge, in contrast to the observations about the cascade endwall flow discussed above. In cascade flows the inlet boundary layer interacts with the airfoil leading edge and most of the boundary layer fluid (normal component of vorticity) gets wrapped up in the horseshoe vortex (streamwise component of vorticity) before any mainstream flow turning occurs. This streamwise component of vorticity is unaffected by the airfoil deflection. The present correlation indicates that the above assumption used in the secondary flow theories may be unrealistic for typical turbine cascades and that the leading edge/inlet boundary layer interaction may be a more important factor than airfoil deflection in determining secondary flow due to the inlet boundary layer.

4 Effect of Inlet Boundary Layer on Cascade Losses

Although a number of cascade tests have been conducted and published in the literature, few of these tests contain enough information about the airfoils tested such as airfoil shapes, airfoil surface static pressure distributions,

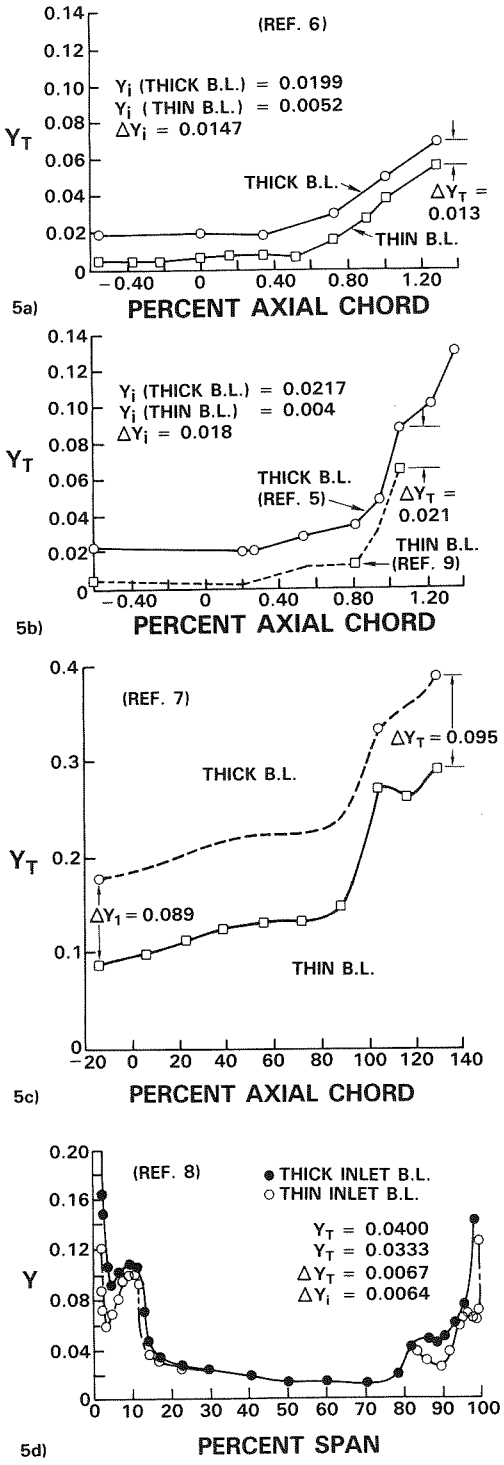

Fig. 5 Loss data from [5–9] indicate that the net cascade passage losses are independent of the cascade inlet boundary layer thickness

measurements of the inlet boundary layer, pitch-averaged exit total pressure profiles, and flow visualization on the airfoil surfaces, to permit detailed analysis of the cascade loss data. Four recently conducted tests, however, do not suffer from the above shortcomings:

(*i*) Tests conducted by Langston et al. [5] and Graziani et al. [9] for a rotor airfoil at low aspect ratio in a large-scale, low-speed rectilinear cascade. These tests were conducted for both thick and thin inlet boundary layers.

(*ii*) Tests conducted by Marchal and Sieverding [6] for both a nozzle and rotor airfoil at high and low Mach numbers

in rectilinear cascades. These tests were conducted at a low aspect ratio for thin and thick inlet boundary layers.

(*iii*) Tests conducted by Gregory-Smith and Graves [7] for a rotor airfoil at an aspect ratio of about two in a large-scale, low-speed, rectilinear cascade. These tests were conducted for three inlet boundary layers.

(*iv*) Tests conducted by Hunter [8] in a large-scale, low-speed annular cascade for a nozzle guide vane. These tests were conducted for two inlet boundary layers.

In the first three of the above tests, measurements of losses were obtained at various axial stations inside the cascade passage including detailed measurements upstream and downstream of the cascade. The development of losses through the cascade for each of these configurations is plotted in Figs. 5(*a–c*) for two test inlet boundary layers. At each station where data are available, the difference in losses between the two tests remains approximately constant and is equal to the difference in loss between the incoming boundary layers. The exit plane pitch-averaged data of Hunter obtained for two inlet boundary layers are shown in Fig. 5(*d*). Here again the difference in loss for the two cases is approximately equal to the difference in inlet boundary layer loss. In each of these four tests the net loss generated inside the passage is approximately the same for both thick and thin inlet boundary layers. This strongly suggests that the inlet losses are additive and that the total loss can be split as follows

$$Y_T = Y_i + Y_{ps} \tag{4}$$

where Y_T = total pressure loss coefficient measured as the difference between the exit total pressure and a reference inlet total pressure; Y_i = inlet loss, contained within the cascade inlet boundary layer; Y_{ps} = passage loss, generated within the passage, this loss is independent of the inlet boundary layer.

A simple expression for the mass-averaged inlet loss can be obtained by integrating the inlet total pressure across the inlet boundary layer assuming the static pressure to be constant to give

$$Y_i = \frac{\delta_1^{**}}{0.5h - \delta_1^*} \frac{\rho_1 U_1^2}{\rho_2 U_2^2} \tag{5}$$

From the discussion in the last sections it is apparent that neither the loss nor the streamwise vorticity attributable to the inlet boundary layer increases as it passes through the cascade passage. This indicates that neither available loss correlations [1–4] nor inviscid secondary flow theories, which relate the amount of secondary loss generated by the inlet boundary layer to the flow turning in the passage, will give physically realistic results for endwall flows in turbine cascades.

It should be noted here that the above conclusions about the effect of inlet boundary layer on turbine cascade secondary flow and loss has been arrived at through the analysis of data obtained for reaction cascades typical of modern high bypass ratio gas turbines used in aircraft transportation. Few detailed data are available for impulse and very low aspect ratio cascades operating with thick inlet boundary layers. In such cases, the inlet boundary layers may have a more pronounced effect on the secondary flows and losses generated in the passage. Until data for such cascades become available the above conclusion cannot be totally generalized.

5 Prediction of Turbine Passage Losses

The losses generated in a turbine passage can be further divided into two components, to facilitate their predictions, as follows

$$Y_{PS} = Y_P + Y_{EW} \tag{6}$$

where Y_P = profile losses and Y_{EW} = endwall secondary flow losses.

The profile losses are generated by the boundary layers developing on the airfoil pressure and suction sides. These losses are independent of the cascade aspect ratio and only for high aspect ratio cascade tests will they be equal to the midheight measured loss. This is because the boundary layers in the midspan regions of cascades are influenced by the endwall secondary flow effects. As pointed out by Dunham [29] and Sharma and Graziani [30], this causes the measured data to be higher than the calculated values. An example of this phenomenon is shown in Fig. 6 where pitch-averaged losses for a cascade test conducted by Langston et al. and Graziani et al. are shown as a function of span. The two sets of data plotted in this figure were obtained at same aerodynamic test conditions except for the thickness of the inlet boundary layer. The total passage losses for these two tests are almost identical as shown in Fig. 5(*a*). If the midspan loses are taken as profile losses, then the thick boundary layer test would yield negative endwall secondary flow losses, which is not physically realistic. Since the measured surface static pressure distributions for both these tests were identical, one would expect the same losses at the midspan. The difference in midspan loss indicates that the endwall secondary flows were affecting the midspan boundary layer development. Measured midspan loss data in almost all cascade tests suffer from the endwall flow effects. Erroneous interpretation of midspan losses as profile losses has invariably resulted in inconsistent estimates of endwall secondary losses from the data and has hindered progress in developing realistic loss prediction models for turbomachinery cascades.

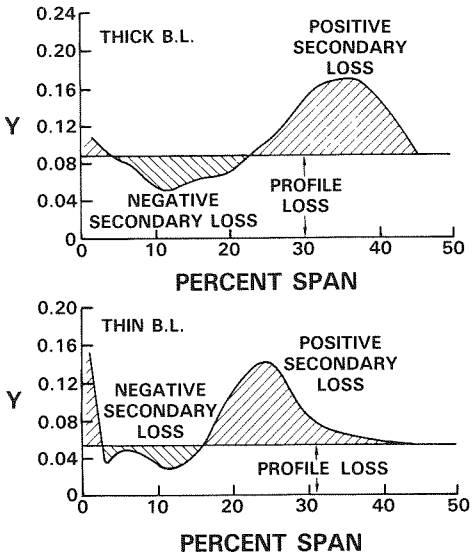

Fig. 6 Data from [5, 9] demonstrate that defining midspan loss as profile loss can result in reduced secondary loss for increased inlet boundary layer thickness

The endwall losses, on the other hand, are generated due to the boundary layer and associated secondary flows in the endwall regions. The procedures adopted in estimating both components of the turbine passage losses are described in the following two subsections.

5.1 Profile Loss Prediction Method. Although a number of correlations are available in published literature for estimating profile losses, as shown by Denton [25] in a review paper, none of these correlations is likely to estimate the profile losses as accurately as boundary layer and mixing calculations conducted for the airfoil pressure distribution as obtained either from measured data or from inviscid flow predictions [26–28].

A number of differential boundary layer calculation methods are available in published literature, for example [30, 31], which can be used to estimate the boundary layer development on turbine airfoils. The method from [30] was used in the present exercise to calculate the two-dimensional boundary

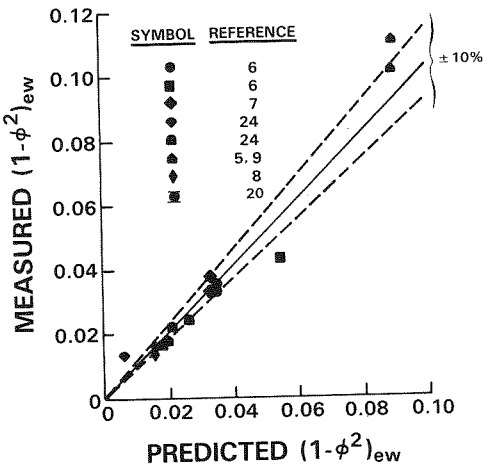

Fig. 7 Predicted endwall losses show good agreement with data

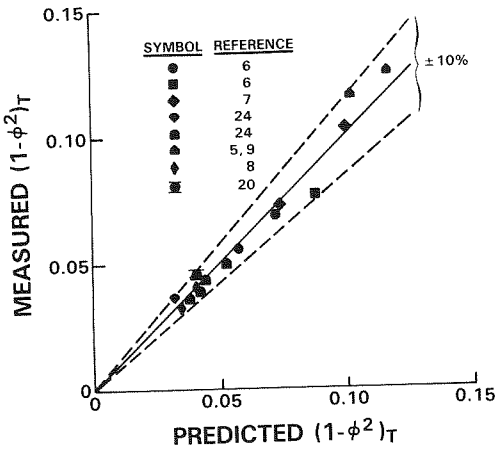

Fig. 8 Predicted total losses show good agreement with data

layer integral parameters, and the mixing analysis developed by Stewart et al. [32] was used to obtain the profile losses for each set of data described below.

5.2 Endwall Secondary Loss Prediction Method. Although in principle a three-dimensional viscous calculation method can be used to estimate endwall secondary losses [13, 14, 33], there is still a need for a semi-empirical model which can be used in the initial design phase of a turbine. Such a semi-empirical model has been developed in the present work by utilizing the classical boundary layer theory developed for the endwall regions of turbomachines. The development of incompressible boundary layer along the pitch-averaged streamline in the endwall regions of a turbine cascade may be written as

$$\frac{d\theta}{ds}+(H+2)\frac{\theta}{U}\frac{dU}{ds}=\frac{C_f}{2} \tag{7}$$

where s = distance along the pitch-averaged streamline; U = pitch-averaged velocity.

θ, H, and C_f are the momentum loss thickness, shape factor, and the skin friction coefficients, respectively, for the boundary layer developing along the pitch-averaged endwall streamline. By using an average value of skin-friction and shape factor in the endwall region and for given velocity and density gradients, equation (7) can be reduced to the following expression for momentum loss thickness at the cascade exit plane

$$\theta_{EW}=S\frac{\overline{C_f}}{2}\left(\frac{U_1}{U_2}\right)^{1+H/2} \tag{8}$$

where $\overline{C_f}$ = average skin friction in the endwall region; U_1/U_2 = ratio of cascade inlet to exit velocity; S = average distance in the endwall region.

Equation (8) can be used to obtain energy loss thickness in the endwall region as

$$\delta^{**}_{EW}=S\frac{\overline{C_f}}{2}H^*\left(\frac{U_1}{U_2}\right)^{1+H/2} \tag{9}$$

Endwall losses can now be obtained by using equation (9) as

$$(1-\theta^2)_{EW}=\frac{2\delta^{**}}{h}=\frac{S}{h}\overline{C_f}\left(\frac{U_1}{U_2}\right)^{1+H/2}H^* \tag{10}$$

An assumption is now made about the behavior of skin friction coefficient for the endwall boundary layer such that it can be obtained by utilizing available correlations from two-dimensional boundary layer theory with a modification to account for the cross flows in the endwall regions. The effect of the crossflow-induced three dimensionality of the boundary layer can be modeled as an extra rate of strain which modifies the skin friction relationship. The proposed relationship for the skin friction may be written as:

$$C_f=C_{f2D}(1+B\mathrm{Ri}) \tag{11}$$

where C_{f2D} = skin friction coefficient for a two-dimensional boundary layer; B = constant; Ri = appropriate Richardson number for endwall boundary layer = $2(Z_{TE}/bx)=0.3\epsilon\sqrt{CR}$.

The above modification to the skin friction is analogous to the ones proposed by Branshaw [34], for flows over curved and/or rotating surfaces and by Sharma and Graziani [30] for convergence and divergence of streamlines. Here the Richardson number has been assumed to be proportional to the magnitude of the endwall secondary flow as obtained from equation (2). The value of constant B in the above equation can be assumed to be of the order of 14 on the basis of analysis conducted in the above two references.

Substituting equation (11) with appropriate values of B and Ri in (10) yields

$$(1-\phi^2)_{EW}=(1+4\epsilon/\sqrt{CR})\frac{S}{h}\overline{C}_{f2D}\left(\frac{U_1}{U_2}\right)^{1+H/2}H^* \tag{12}$$

The above equation can be simplified as

$$(1-\phi^2)_{EW}=(1+4\epsilon/\sqrt{CR})2\frac{\delta^{**}_{2D}}{h} \tag{13}$$

where $\delta^{**}_{2D}=H^*\overline{SC}_{f2D}(U_1/U_2)^{1+H/2}$; δ^{**}_{2D} = energy loss thickness for two-dimensional boundary layer developing over the endwall surface in the absence of crossflows.

The δ^{**}_{2D} can also be obtained by using two-dimensional boundary layer loss on the airfoil pressure and suction surfaces, as

$$\delta^{**}_{2D}=(1-\phi^2)_{2D}\frac{\tau\sin\beta_2-\mathrm{TET}}{2} \tag{14}$$

where $(1-\phi^2)_{2D}$ = energy loss coefficient for profile losses; H^* = shape factor based on energy deficit thickness.

Substituting equation (14) into equation (13) results in the following expression for endwall losses

$$(1-\phi^2)_{ew}=(1-\phi^2)_{2D}\frac{\tau\sin\beta_2-\mathrm{TET}}{h}\left(1+4\frac{\epsilon}{\sqrt{CR}}\right) \tag{15}$$

The total losses generated in the cascade passage can now be given as

$$(1-\phi^2)_{ps}=(1-\phi^2)_{2D}+(1-\phi^2)_{EW}$$
$$=(1-\phi^2)_{2D}\left[1+\left(1+\frac{4\epsilon}{\sqrt{CR}}\right)\frac{\tau\sin\beta_2-\mathrm{TET}}{h}\right] \tag{16}$$

To demonstrate the predictive capability of equation (15)

for endwall secondary loss, several turbine cascade data sets were analyzed [5–9, 20, 24]. These data consisted of the spanwise distribution of total pressure loss at inlet and exit of the cascade and knowledge of the airfoil midspan surface pressure distribution either from measurement or from inviscid flow calculation, cascade geometry, and test conditions. All of the abovementioned experimental investigations were conducted at near design incidence and loss data were acquired at about 0.5 axial chord downstream of the cascade trailing edge by which time most of the mixing losses have occurred. The major contribution to the mixing losses occur because of dissipation of the secondary flow vortex [35]. In the present model the mixing losses are assumed to be proportional to the secondary loss and these are included in the losses predicted by equation (15).

The proposed method of splitting the total loss allowed the endwall loss to be extracted from this data. The inlet loss was obtained from the measured inlet boundary layer by using equation (5) or from the data if measured directly. Where only the boundary layer thickness was available a power law exponent equal to 5 was assumed to obtain the energy and displacement thicknesses. The two-dimensional profile loss was obtained using the method described in Section 5.1. The input to this boundary layer calculation was the measured midspan pressure distribution when available or the results from an inviscid flow solver [27] when data were unavailable. Subtracting the sum of inlet loss and two-dimensional profile loss from the total loss gave the endwall secondary loss.

A comparison of the measured endwall secondary loss with the loss calculated using equation (15) is shown in Fig. 7. It should be pointed out here that the present procedure deduced endwall secondary losses from measured total losses, thus errors in estimation of profile and inlet losses appear as errors in the prediction of endwall secondary losses. A more realistic evaluation of the present procedure is a comparison between the measured and predicted total losses. Predictions for total loss obtained by adding the inlet loss and the two-dimensional profile loss (as calculated from the method described in section 5.1) to the endwall secondary loss are shown in Fig. 8 compared to the total loss data. Most of the data fall within a ± 10 percent scatter band which must be considered to be within the accuracy of the data for these types of measurement.

6 Conclusions

A method has been described for estimating secondary flows and endwall losses for axial flow turbomachine cascades. Detailed study of available experimental cascade data indicates that the effect of inlet boundary layer as predicted by classical secondary flow theories is incorrect for typical turbomachine configurations because the formation of the leading edge horseshoe vortex transforms incoming normal vorticity to streamwise vorticity independent of flow turning. A simple expression is given which accurately predicts the spanwise extent of the secondary flow region at the trailing edge in terms of meanline geometric parameters and inlet boundary layer thickness. Analysis of cascade loss data has demonstrated that inlet boundary layer losses convect through the passage without causing additional loss and can be distinguished from the passage loss. The passage loss can then be split into a two-dimensional profile loss and an endwall secondary loss. The two-dimensional profile loss can be calculated using an accurate two-dimensional boundary layer calculation method which accounts for the transitional nature of the airfoil boundary layer in the detailed design phase, or it can be correlated to the meanline loading for use in the preliminary design phase. A semi-empirical expression is given for endwall secondary loss based on pitch-averaged boundary layer concepts where the extra rate of strain associated with three dimensionality of the boundary layer is assumed proportional to the spanwise extent of the secondary flow region at the trailing edge. The resulting expression for secondary loss combined with the two-dimensional profile loss calculated using a boundary layer calculation method and the inlet loss gives predictions for cascade losses within ± 10 percent of measured losses.

References

1 Dunham, J., "A Review of Cascade Data on Secondary Losses in Turbine," *Journal of Mechanical Engineering Sciences*, Vol. 12, 1970, pp. 48–59.

2 Came, P. M., "Secondary Loss Measurements in a Cascade of Turbine Blades," Institute of Mechanical Engineers, Conference Publication No. 3, 1973.

3 Dunham, J., and Came, P. M., "Improvements to the Ainley–Mathieson Method of Turbine Performance Prediction," ASME JOURNAL OF ENGINEERING FOR POWER, Vol. 92, July 1970.

4 Morris, A. W. H., and Hoare, R. G., "Secondary Loss Measurements in a Cascade of Turbine Blades With Meridional Wall Profiling," ASME Paper No. 75-WA/GT-13.

5 Langston, L. S., Nice, M. L., and Hooper, R. M., "Three-Dimensional Flow in a Turbine Cascade Passage," ASME JOURNAL OF ENGINEERING FOR POWER, Vol. 99, 1977, pp. 21–28.

6 Marchal, P. H., and Sieverding, C. H., "Secondary Flows Within Turbomachinery Bladings," *Secondary Flow in Turbomachines*, AGARD CP No. 214, 1977, Paper No. 11.

7 Gregory-Smith, D. G., and Graves, C. P., "Secondary Flows and Losses in a Turbine Cascade," *Viscous Effects in Turbomachines*, AGARD CP No. 351, 1983, Paper No. 17.

8 Hunter, I. H., "Endwall Boundary Layer Flows and Losses in Axial Turbomachines," Ph.D. Thesis, University of Cambridge, 1979.

9 Graziani, R. A., Blair, M. F., Taylor, J. R., and Mayle, R. E., "An Experimental Study of Endwall and Airfoil Surface Heat Transfer in a Large Scale Turbine Blade Cascade," ASME JOURNAL OF ENGINEERING FOR POWER, Vol. 102, 1980, pp. 257–267.

10 Sieverding, C. H., "Recent Progress in the Understanding of Basic Aspects of Secondary Flows in Turbine Blade Passages," ASME JOURNAL OF ENGINEERING FOR GAS TURBINES AND POWER, Vol. 107, 1985, pp. 248–257.

11 Gregory-Smith, D. G., "Secondary Flows and Losses in Axial Flow Turbines," ASME JOURNAL OF ENGINEERING FOR POWER, Vol. 104, 1982, pp. 819–822.

12 Mukhtarov, M. Kh., and Krichakin, V. I., "Procedure for Estimating Flow Section Losses in Axial Flow Turbines When Calculating Their Characteristics," *Teploenergetika*, Vol. 18, 1969, pp. 76–79.

13 Dodge, P. R., "Numerical Method for 2-D and 3-D Viscous Flows," *AIAA Journal*, Vol. 15, 1977, pp. 961–965.

14 Hah, C. H., "A Navier–Stokes Analysis of Three-Dimensional Turbulent Flows Inside Turbine Blade Rows at Design and Off-Design Conditions," ASME JOURNAL OF ENGINEERING FOR GAS TURBINES AND POWER, Vol. 106, 1984, pp. 421–429.

15 Squire, H. B., and Winter, K. G., "The Secondary Flow in a Cascade of Airfoils in a Non-uniform Stream," *Journal of Aero Sciences*, Vol. 18, 1951.

16 Hawthorne, W. R., "Secondary Circulation of Fluid Flow," *Proceedings of Royal Society A*, Vol. 203, 1951.

17 Horlock, J. H., and Lakshminarayana, B., "Secondary Flows: Theory, Experiments and Application in Turbomachinery Aerodynamics," *Annual Review of Fluid Mechanics*, 1973, pp. 247–280.

18 Smith, L. H., "Secondary Flow in Axial-Flow Turbomachinery," *ASME Transactions*, 1955, pp. 1065–1076.

19 Lakshminarayana, B., "Effect of Inlet Temperature Gradients on Turbomachinery Performance," ASME JOURNAL OF ENGINEERING FOR POWER, Vol. 99, 1975, pp. 64–74.

20 Kopper, F. C., Milano, R., and Vanco, M., "An Experiment Investigation of Endwall Profiling in a Turbine Vane Cascade," *AIAA Journal*, Vol. 19, Aug. 1981.

21 Barber, T. J., and Langston, L. S., "Three-Dimensional Modeling of Cascade Flows," AIAA Paper No. 79-0047, Jan. 1979.

22 Kopper, F. C., private communication.

23 Bindon, J. P., "Exit Plane and Suction Surface Flows in an Annular Turbine Cascade With a Skewed Inlet Boundary Layer," *International Journal of Heat and Fluid Flow*, Vol. 2, 1980, pp. 57–66.

24 Sharma, O. P., Kopper, F. C., Knudsen, L. K., and Yustinich, J. B., "Low Pressure Turbine Subsonic Cascade Technology Report – Energy Efficient Engine Component Development and Integration Program," NASA CR-165592, PWA 5594-167, 1982.

25 Denton, J. D., "A Survey and Comparison of Methods for Predicting the Profile Loss of Turbine Blades," Inst. Mechanical Engineering Conference, Publication 3, C76/73, 1973.

26 Denton, J. D., "A Time Marching Method of Two and Three-Dimensional Blade to Blade Flows," ARC, R&M #3775, 1974.

27 Caspar, J. C., Hobbs, D. G., and Davis, R. L., "The Calculation of Two-Dimensional Compressible Potential Flow in Cascades Using Finite Area Techniques," AIAA Paper No. 79-0007, Jan. 1979.

28 Ri, R. H., "A Multiple-Grid Scheme for Solving the Euler Equations," *AIAA Journal*, Vol. 20, Nov. 1982.

29 Dunham, J., "The Effect of Stream Surface Convergence on Turbomachine Blade Boundary Layers," *Aeronautical Journal*, 1974, pp. 90–92.

30 Sharma, O. P., and Graziani, R. A., "Influence of Endwall Flow on Airfoil Suction Surface Midheight Boundary Layer Development in a Turbine Cascade," ASME JOURNAL OF ENGINEERING FOR POWER, Vol. 105, 1983, pp. 147–155.

31 McDonald, H., and Fish, R. W., "Practical Calculations of Transitional Boundary Layers," *International Journal of Heat and Mass Transfer*, Vol. 16, 1971, pp. 1729–1744.

32 Stewart, E. L., "Analysis of Two-Dimensional Compressible Flow Loss Characteristics of Turbine Blades in Terms of Basic Boundary Layer Parameters," NACA TN 3515, 1955.

33 Rhie, C. M., "A Pressure Based Navier–Stokes Solver Using the Multigrid Method," AIAA Paper No. 86-0207, Jan. 1986.

34 Bradshaw, P., "The Analogy Between Streamline Curvature and Buoyancy in Turbulent Shear Flow," *Journal of Fluid Mechanics*, Vol. 36, 1969.

35 Moore, J., and Adhye, R. Y., "Secondary Flows and Losses Downstream of a Turbine Cascade," ASME JOURNAL OF ENGINEERING FOR GAS TURBINES AND POWER, Vol. 107, 1985, pp. 961–968.